Chemical Engineering Journal 227 (2013) 116–127

Contents lists available at SciVerse ScienceDirect

Chemical Engineering Journal

journal homepage: www.elsevier.com/locate/cej

Mixing performance assessment of a multi-channel mini heat exchanger reactor with arborescent distributor and collector

Xiaofeng Guo, Yilin Fan, Lingai Luo *

Laboratoire Optimisation de la Conception et Ingénierie de l'Environnement (LOCIE), CNRS UMR 5271, Université de Savoie, Campus Scientifique, Savoie Technolac, 73376 Le Bourget du Lac CEDEX, France

HIGHLIGHTS

- A design of mini-scale, multi-channel heat exchanger reactor is proposed.
- Rapid mixing is observed by using visualization and competitive reactions.
- Comparable mixing performance is obtained with that of several micro-structured designs.
- Arborescent structure provides uniform distribution for the numbering-up of channels.

ARTICLE INFO

Article history:
Available online 30 August 2012

Keywords:
Heat exchanger reactor
Arborescent distributor and collector
Micromixing
Process intensification
Iodide/iodate reaction

ABSTRACT

A mini reactor with 16 channels and with channel diameter of 1 mm or 2 mm is designed, fabricated and studied experimentally. Two fluids are divided into 16 channels through distributor, then contacted at T-mixers, and finally collected. Both distributor and collector are designed following the arborescent shape. Visualization with pH indicator bromothymol blue (BTB) is used to qualitatively observe the global mixing; while for the micromixing performance assessment, we used competitive iodide/iodate (Villermaux/Dushman) reactions. Segregation index and micromixing time, with respect to energy dissipation rate are used to characterize micromixing performance.

Visualization with pH indicator shows that complete global mixing at the collector by liquid impingement is obtained under our tested conditions. Iodide/iodate reaction shows a rapid mixing at molecular level as the flowrate increases and impingement being enhanced. Micromixing time estimated by IEM (Interaction by Exchange with the Mean) model is compared with other micro-structured mixers in the literature. Comparable mixing performance is obtained using our millimetric reactor with that of micro-structured designs.

The design of multi-channel reactor with arborescent distributor and collector makes possible the numbering-up of multiple channels. Process intensification is highlighted by high throughput and compact size, thus may be attractive for industrial application.

© 2012 Elsevier B.V. All rights reserved.

1. Introduction

Process intensification, particularly the design of high yield processes or compact equipments in the field of process engineering, has become one of the pressing industrial needs in recent years. Paths leading to intensification include the miniaturization of process equipment, system integration of multiple devices or processes, etc. [1–4]. Similarly, *continuous processing* is preferable for designing future processes. It ranked on the first of the Top 10 green engineering research areas in pharmaceutical industry summarized by American Chemical Society Green Chemistry Institute in 2007 [5]. Together with inline analysis, continuous processing provides high safety and quality control in many areas of chemical and process engineering.

One of the routes to reach both process intensification and continuous processing is the use of mini/microscale equipments. Reactors with mini/microchannels enhance heat and mass transfer characteristics mainly due to their high surface/volume ratio. One important issue for industrializing their application is the numbering-up problem. Currently most researches about mini/microchannel reactor end up with single channel study. Several studies have used multi-channels to gain throughput, however only a few researches take into account of the flow maldistribution problem [6–12]. Nonuniform flow among channels is usually a main cause of performance deterioration or malfunction of these

* Corresponding author. Tel.: +33 4 79 75 81 93; fax: +33 4 79 75 81 44.
E-mail address: Lingai.LUO@univ-savoie.fr (L. Luo).

1385-8947/$ - see front matter © 2012 Elsevier B.V. All rights reserved.
http://dx.doi.org/10.1016/j.cej.2012.08.068

Nomenclature

C	concentration (mol/L)
ϵ	energy dissipation rate (W/kg)
ϵ_{353}	extinction coefficient at 353 nm for tri-iodide (L/(mol cm))
e	fitting exponent
I	ionic strength (mol/L)
k	kinetic constant
l	length of light path (cm)
n	molar quantity (mol)
OD	optical density, spectrophotometric absorption (a.u.)
ΔP	pressure loss (bar)
Q	volume flowrate (mL/min)
t	time (s)
V	internal volume of reactor (m^3)
V_m	mixing volume in reactor (m^3)
X_S	segregation index
Y	selectivity of acid consumption
Z	ionic charge

Indices

0	initial
1	reactor with channel diameter 1 mm, M1
2	reactor with channel diameter 2 mm, M2
diss	energy dissipation
m	mean, mix
macro	macro-observation
micro	micromixing
ST	total segregation

devices. As a result, how to propose novel designs of multi-channel mini/micromixer-reactors with uniform flow distribution between channels receives more and more attention in recent years.

Mixing is one of the most important steps to conduct a high yield reaction. Especially for some fast reactions, rapid mixing ($t_{mixing} < t_{reaction}$) is crucial to obtain high chemical selectivity. Mixing process can be categorized into macro-, meso- and micromixing according to their mechanisms and dimensional scale [13,14]. Macromixing by fluid turbulence is the first step, which happens usually in the scale of whole equipment; the second step, mesoscale mixing, is driven by fluid viscosity or shear stress between fluids or fluid-wall surfaces; and the final step is micro-scale mixing driven by diffusion of molecules. The whole mixing process happens with three mixing in a cascade manner (macro to meso to micro). Particularly the micro-scale mixing is essential for chemical processes because it relates directly with molecular exchange.

Different methods have been developed by researchers to assess mixing performance. In general mixing characterization methods could be sorted by either direct flow visualization or chemical reaction method. Particles with PIV (Particle Image Velocimetry) system, fluorescence with microscopy or LIF (Laser Induced Fluorescence) method, etc., have been used as tools to observe flow field in transparent prototypes [13,15–18]. Chemical reaction methods mainly involve several competitive reactions whose selectivity is sensitive to mixing. Typical chemical schemes are iodide/iodate reaction [19,20], diazo coupling reaction [21–23], Walker scheme [24–26], etc. The last two reaction schemes are related with thermal treatment because reactions are either exothermic or endothermic. Among the methods above, only chemical reactions can reflect mixing down to microlevel. A detailed review of mixing assessment methods was given by Aubin et al. [27] recently.

Among various micromixing characterization methods, iodide/iodate reaction scheme [28] (or Villermaux/Dushman reaction) is well adapted and widely used. Kinetic data of reactions are well-known so that it is easy to analyze the results quantitatively. A simple model to characterize micromixing process is IEM (Interaction by Exchange with the Mean) model, developed by Villermaux and Falk [29]. Using this model micromixing time can be related with experimental results from iodide/iodate reaction. Recent literature reviews on micromixing performance assessment are presented by Falk and Commenge [30,31] by employing this model on different experimental results.

In this paper, we propose an integrated design of a mini-scale, multi-channel mixer-reactor. Arborescent style distributor is used to achieve uniform fluid distribution among channels. Two fluids are contacted at 16 T-junctions and complete the mixing within channels and in arborescent collector. Heat exchanger, mixer and reactor are integrated together in this continuous processing equipment.

Firstly pH sensitive dye BTB (bromothymol blue) is used as color indicator to visualize the mixing and flow behaviors inside our reactor. Then competitive iodide/iodate reaction with IEM model are implemented to quantitatively explore the micromixing performance of the proposed reactor. Finally a performance comparison between our designs and other micro-structured mixer/reactors is made, in terms of micromixing time and energy dissipation.

2. Heat exchanger reactor design and geometry

The application of multi-scale, nature-inspired structures for fluid distribution and collection has been studied extensively [32–38] during the last decade. Scaling relations were established analytically by Luo and Tondeur [32,33] for the design of multi-scale distributor/collectors, considering energy dissipation and fluid distribution uniformity. Multi-scale components with arborescent internal structures, i.e. distributor/collector, heat exchanger, mixer and their integrations have been designed and investigated [35,36,38].

Based on the experiences above, we developed a multi-functional heat exchanger reactor, integrating heat exchanger, mixer and reactor. Shown in Fig. 1a is the whole geometry, including arborescent structures used for connecting single inlet/outlet and multiple parallel channels. In general we have two inlets of different fluids to be mixed and one outlet for product. Two fluids of each inlet are injected and then distributed into 16 channels. The two fluids then contact through T-junctions where mixing happens with counter-current impingement. After, the mixture goes along the channels to gain complete mixing. The final mixture will then be collected to the outlet. Symmetry design of this nature-inspired distributing/collecting structure makes the flow path of fluid in every channel being identical. Non-uniformity of flow distribution between channels is minimized.

For clarity we define number 0–4 to represent different channel scales in arborescent structure, i.e., 0 representing the lowest scale (each of 16 branches) and 4 representing the highest (main outlet for the case of collector, as indicated later in Fig. 6a).

Heat exchange chamber is located outside the vertical parallel channels. Inlet and outlet are arranged in such a way that utility fluid flows reversely with inside fluid. Counter-current flow is essential for an efficient heat transfer for this shell-and-tube heat

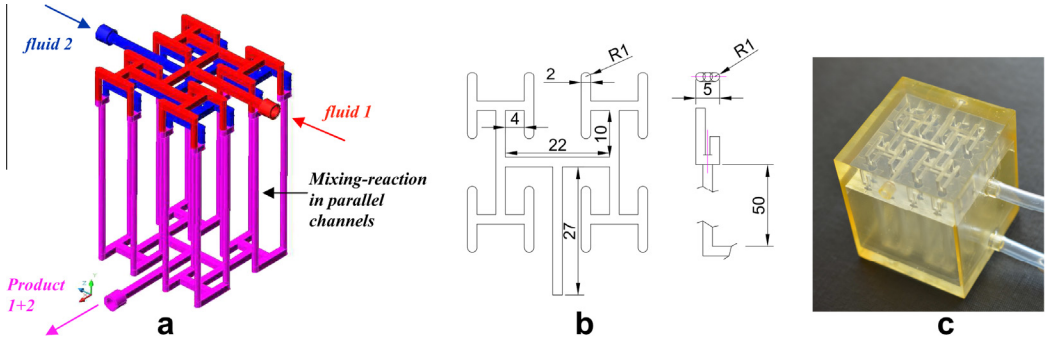

Fig. 1. Design and dimension of multifunctional exchanger. ((a) Design of multi-channel reactor with arborescent distributor and collector; (b) dimension of distribution and channel; and (c) photo of the resin fabricated prototype M2) (unit:mm).

exchanger. Precise temperature control for endothermic and exothermic reactions is expected by the integration of heat exchanger in the reactor.

Two different sizes of reactor are studied here. One has a channel diameter of 2 mm, as described in Fig. 1b and c. The other reactor is more compact with its channel diameter being 1 mm. For clarity we named them as M1 (diameter 1 mm) and M2 (diameter 2 mm), respectively. For better visualization of the flow field, the cross-section of all channels of distributors and collector is square shape (2 mm × 2 mm for M2 and 1 mm × 1 mm for M1), as indicated in Fig. 1a. Total internal volume of reactor M1 and M2 is 1.27 mL and 6.07 mL, respectively.

Prototypes of the two reactors were fabricated using stereolithography method. The small reactor M1 was fabricated with metal powder Cobalt-Chrome, while the big one M2 was fabricated with transparent resin. Metal made M1 can be used for heat exchange test by obtaining an efficient heat transfer between the tube-side and shell-side. Another advantage of M1 is that it resists high temperature. Whereas with the transparent feature of M2, we are able to visualize the internal flow behaviors with optical tracer and fast camera.

3. Global mixing visualization with pH indicator

We use pH sensitive indicator BTB (bromothymol blue) and a color camera to qualitatively observe the mixing and flow inside the transparent reactor M2. BTB appears yellow in acidic solutions (pH < 6.0) whilst blue in basic solutions (pH > 7.6). In neutral solution, it looks bluish green.

Preparation procedure and solution concentrations are in accordance with the study by Kockmann et al. [39]. Solution 1 is comprised of 1.5×10^{-3} mol/L BTB (Analytic level, Bioblock France) with lab deionized water, showing pH = 5.9. Solution 2 is 6.7×10^{-2} mol/L Na_2HPO_4 (Disodium hydrogen phosphate, Analytic level, Bioblock France) in deionized water, showing pH = 9.0 in our case. Solution 1 shows a color of light yellow while solution 2 is colorless. The 1:1 volumetric mixture of the two solution results in a color of blue with solution pH > 8. A color camera was positioned above the reactor to monitor the color evolution of the collector region.

3.1. Global mixing time estimation

Through the homogeneity of color, we could estimate the locations from which two fluids are completely homogeneous at macro-scale. We consider that the color-changing time for BTB at our condition is negligible compared to the global mixing time. Actually this assumption is reasonable since Kockmann et al. [39] succeeded in measuring a mixing time of several milliseconds, which is much smaller than our case.

Global mixing time thus could be calculated easily with known geometric volume and total volumetric flowrate Q (m^3/s):

$$t_{m,macro} = \frac{V_m}{Q} \tag{1}$$

where V_m is the volume passed by liquid starting from the T-mixer to fully mixed point. The subscript *macro* indicates that the result is obtained through macro-observation, other than micromixing assessment using chemical reaction method.

It has to be noted that this observation of fluid mixing is in macro-scale since it is obtained only through camera observation. The estimated mixing time represents the time needed to achieve macro-scale mixing.

3.2. Energy dissipation rate

Pressure drops for prototypes were measured using pressure gauge (SEN-3247 membrane sensor, 0–1 bar, ±0.1% precision, KOBOLD Messring GmbH). Measuring point is placed close to the reactor inlet to minimize the influence of tubing. At the outlet liquid runs out directly to a drain. Pressure drops at various flowrates (flowrate is measured by weighing method using a digital balance and a stopwatch) are studied.

To compare the hydraulic performance with that of other designs in the literature, energy dissipation rate ϵ (W/kg) is introduced (Eq. (2)). This parameter shows the energy required to pump a mass unit of standard fluid (water), through the mixer-reactor [40].

$$\epsilon = \frac{Q\Delta P}{\rho V} \tag{2}$$

where V is the internal volume of reactor, m^3; ΔP the pressure loss measured between the inlet and outlet, Pa; and ρ the density of test fluid.

Different from pressure loss, which depends largely on working conditions and number of modules, energy dissipation rate reflects directly the energy consumption for one kilogram of product. This parameter is then more adaptive for performance comparison.

For Hagen–Poiseuille flow in a pipe, theoretical energy dissipation rate can be calculated as:

$$\epsilon = \frac{512 v Q^2}{\pi^2 d^6} \tag{3}$$

where v is the kinematic viscosity, m^2/s; and d the pipe diameter, m.

4. Micromixing characterization with iodide/iodate reaction

Competitive iodide/iodate reaction is used in this study to evaluate the micromixing performance of our design. This reaction scheme is sensitive to mixing in molecular level by the production of iodine (I_2). Two proton-competing parallel reactions include a neutralization reaction (R1) and a redox reaction (R2).

$$H_2BO_3^- + H^+ \rightarrow H_3BO_3 \quad \text{quasi} - \text{instantaneous} \tag{R1}$$

$$5I^- + IO_3^- + 6H^+ \rightarrow 3I_2 + 3H_2O \quad \text{very fast} \tag{R2}$$

$$I_2 + I^- \rightleftharpoons I_3^- \quad \text{quasi} - \text{instantaneous} \tag{R3}$$

Basic principle of iodide/iodate reaction is shown in Fig. 2. The selectivity of parallel reactions depends strongly on mixing characteristic time and reaction time. Globally excessive $H_2BO_3^-$ could consume H^+ rapidly since the reaction (R1) is quasi-instantaneous. However at molecular level, locally excessive H^+ may contact with iodide and iodate ions. This will produce iodine in an irreversible manner. Redox reaction is comparatively slower than the neutralization reaction. However both reactions are much faster than the mixing for current study.

With the existence of iodide ions, a part of iodine could yield triiodide ions through equilibrium reaction (R3). Iodide, iodine and tri-iodide all exist in the final solution complex. The tri-iodide ion shows absorption peaks to ultraviolet (UV) light at wavelength of 286 nm and 353 nm, respectively. Its concentration then could be determined quantitatively by employing a spectrophotometer.

4.1. Reactions kinetics

Kinetics for each reaction are well known [41,42] and can be described as:

$$r_1 = k_1 C_{H^+} C_{H_2BO_3^-}$$

$$r_2 = k_2 C_{H^+}^2 C_{I^-}^2 C_{IO_3^-}$$

$$r_3 = k_{3+} C_{I^-} C_{I_2} - k_{3-} C_{I_3^-}$$

where k represents the kinetics constant of each reaction. (R1) is a second order reaction while (R2) is fifth order, and (R3) is an equilibrium reaction.

As a neutralization reaction, (R1) is quasi instantaneous with its rate constant being calculated as follows:

$$log_{10}(k_1) = \text{pK}\left(\frac{H_3BO_3}{H_2BO_3^-}\right) = 9.2 \tag{4}$$

For reaction (R2) the kinetics constant depends on ionic strength I of the mixture, they are related by:

$$log_{10}(k_2) = \begin{cases} 9.28105 - 3.664\sqrt{I} \text{ for } I < 0.166 \text{ mol/L} \\ 8.38300 - 1.5112\sqrt{I} + 0.237I \text{ for } I \geqslant 0.166 \text{ mol/L} \end{cases} \tag{5}$$

Ionic strength can be calculated by multiplying the molar concentrations C_i and charges Z_i of each species in solution and then summarizing them. It is given by:

$$I = \frac{1}{2}\sum C_i Z_i^2 \tag{6}$$

here i denotes all ion species in the solution.

For equilibrium reaction (R3), kinetic data at 25 °C are [43,44]:

$$k_{3+} = 5.9 \times 10^9 \text{ L/(mol s)}$$

$$k_{3-} = 7.5 \times 10^6 \text{ s}^{-1}$$

The equilibrium of the iodine–iodide–triiodide complex is defined by constant K_{eq}, which is determined by the ratio of forward rate constant k_{3+} and reverse rate constant k_{3-}. When species concentrations stop changing in the solution, we have:

$$K_{eq} = \frac{C_{I_3^-}}{C_{I_2} C_{I^-}} \tag{7}$$

To relate the equilibrium constant with reaction condition, study by Palmer et al. [45] gives:

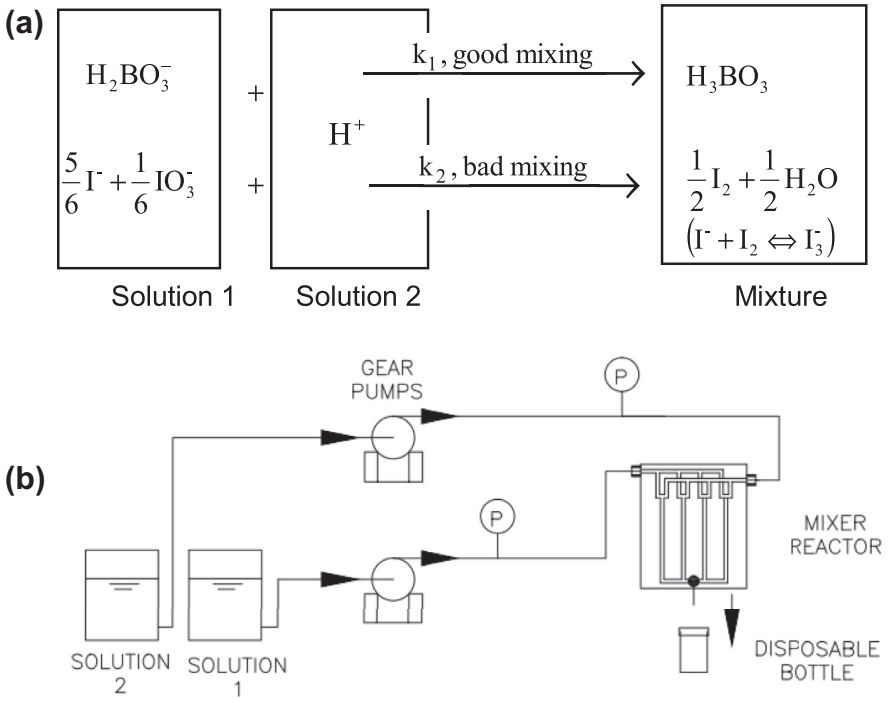

Fig. 2. Chemical principle and experimental setup of competitive reactions; (a) competitive mechanism of neutralization reaction and redox reaction, and (b) Schematic of the experiment setup.

$$\log_{10}K_{eq} = \log_{10}\frac{k_{3+}}{k_{3-}} = \frac{555}{T} + 7.355 - 2.575\log_{10}T \quad (8)$$

where T is temperature in K. At 25 °C this constant K_{eq} is 698 L/mol. Final product of I_3^-, I_2 and I^- can thus be determined by kinetic equations.

4.2. Beer Lambert Law

Quantification of the tri-iodide ions could be done by employing the Beer-Lambert Law. This law relates spectrometric absorption (a.u.) with concentration by several parameters as follows [28,30]:

$$C_{I_3^-} = OD/\epsilon_{353}l \quad (9)$$

where OD denotes the optical density or absorbance through the cuvette, a.u.; l stands for the optical path length, here l = 1 cm, which is the dimension of standard spectrometric optical cuvette; ϵ_{353} is the extinction coefficient for tri-iodide ions at 353 nm, ϵ_{353} = 26047 L/(mol cm).

4.3. Segregation index

We use segregation index (X_S) to characterize the micromixing performance. X_S, as defined by Eq. (10), can be calculated by the ratio of iodine production in the experiment and that in total segregation case (when mixing is infinitely slow). The production of iodine could be represented by consumption of acid during reaction. Value of segregation index lies within 0 and 1, where X_S = 1 stands for two fluids totally segregated while X_S = 0 means infinitely fast mixing in molecular level.

$$X_S = \frac{Y}{Y_{ST}} \quad (10)$$

where Y is the ratio of the side reaction (R2) consumption of acid to the whole consumption of acid by (R1) and (R2), and Y_{ST} is the value of Y in the case of total segregation.

In the case of total segregation, and with the presence of sufficient ions of iodide, all the ions of Iodate will be consumed by reaction (R2). The selectivity of acid thus can be calculated as:

$$Y_{ST} = \frac{6n_{IO_3^-,0}}{6n_{IO_3^-,0} + n_{H_2BO_3^-,0}} = \frac{6C_{IO_3^-,0}Q_1}{6C_{IO_3^-,0}Q_1 + C_{H_2BO_3^-,0}Q_1} \quad (11)$$

where n stands for molar number (mol) and C the concentration (mol/L); subscript 0 means that concentrations are initial values in one solution other than in the mixture; and subscripts 1 and 2 indicate the two solutions S1 and S2.

During an experimental test, the selectivity of acid could be calculated with the ratio of acid consumed to produce iodine, with the total amount of hydrogen ions from sulfuric acid. It has to be noted that tri-iodide ions which are produced by equilibrium reaction (R3), should be considered together with iodine I_2. Thus we have:

$$Y = \frac{2\left(n_{I_2} + n_{I_3^-}\right)}{n_{H_0^+}} = \frac{2(C_{I_2} + C_{I_3^-})(Q_1 + Q_2)}{2C_{H_2SO_4}Q_2} \quad (12)$$

in which the subscript 0 should be carefully treated since it is the initial concentration before mixing.

In our study we keep an identical volume flowrates $Q_1 = Q_2$. Y and Y_{ST} could then be simplified so that both of them depend only on concentrations:

$$Y_{ST} = \frac{6C_{IO_3^-,0}}{6C_{IO_3^-,0} + C_{H_2BO_3^-,0}} \quad (13)$$

$$Y = \frac{2\left(C_{I_2} + C_{I_3^-}\right)}{C_{H_2SO_4}} \quad (14)$$

The next step is to relate the production of iodine with the concentration of tri-iodide ions. This requires combining the equilibrium kinetics of (R3) with the mass balance of iodine (I) in (R2).

Mass balance of iodine (I) for the reaction (R2) can be written as:

$$n_{I^-} = n_{I^-,0} - \frac{5}{3}\left(n_{I_2} + n_{I_3^-}\right) - n_{I_3^-} \quad (15)$$

where $n_{I^-,0}$ stands for the initial mole of iodide before reaction in solution 1.

$$C_{I^-}(Q_1 + Q_2) = C_{I^-,0}Q_1 - \frac{5}{3}\left(C_{I_2} + C_{I_3^-}\right)(Q_1 + Q_2) - C_{I_3^-}(Q_1 + Q_2) \quad (16)$$

We could derive the final mass balance for iodine by Eq. (15):

$$C_{I^-} = \frac{C_{I^-,0}}{2} - \frac{5}{3}\left(C_{I_2} + C_{I_3^-}\right) - C_{I_3^-} \quad (17)$$

Combining the equilibrium equation Eq. (7) and the mass balance equation Eq. (17), final concentration of iodine could be calculated easily with measured concentration of tri-iodide:

$$-\frac{5}{3}C_{I_2}^2 + \left(\frac{C_{I^-,0}}{2} - \frac{8}{3}C_{I_3^-}\right)C_{I_2} - \frac{C_{I_3^-}}{K_{eq}} = 0 \quad (18)$$

The segregation index X_S could then be calculated by Eqs. 10, 13 and 14.

4.4. Experiment procedure and uncertainty

Preparation of solution iodate–iodide–borate (S1) was kept in such a sequence that no redox reaction happens inside the solution complex. NaOH and boric acid solutions were mixed firstly to produce $H_2BO_3^-$, and then KI and KIO_3 were added. Coexistence of I^- and IO_3^- can only be kept following this procedure. Concentrations of solutions are listed in Table 1.

Two gear pumps (max. 2000 mL/min, Diener Precision Pump Ltd.) were used to deliver the two solutions. Flowrates can be easily adjusted by varying the input voltage and thus the motor speed. A digital balance (KERN EW 4200-2NM, max. 4200 g, precision ±0.1 g) and a stopwatch were used to calibrate the relation between motor speed and flowrate. Products were collected with single-use bottles.

Absorption tests for quantifying the concentration of tri-iodide were done by a UV–Visible spectrophotometer (HACH LANGE DR3900, software version 1.3), within standard plastic spectra cuvettes (1 cm optical path, disposable). The same type of cuvette with deionized water was used as reference between each analysis.

All reactants are of analytical level and were bought recently. Lab deionized water was used for solution diluting. Experiments were implemented within 6 h after solution preparation to avoid influence from ambient temperature, light, etc. Each set of experiments was implemented carefully with a repetition of at least three times. Room temperature was about 22–24 °C during the experiment.

Precision of the spectra absorption measurements may not be influenced by the time between sampling and offline spectrometric analysis. To confirm this assumption, spectrometric analyses were carried out to the same sample but with a difference of 24 h

Table 1
Reagents and their concentrations in each solution.

Solution 1 (mol/L)	Solution 2 (mol/L)
NaOH:0.125 H_3BO_3:0.25 KI:0.0116 KIO_3:0.00233	H_2SO_4:0.036

between two analyses. A difference within 12% (0.61 a.u. v.s. 0.54 a.u.) was found between the two results. Inaccuracy arising from a time difference of maximum 30 min between reaction and spectra analysis in our case may thus be considered negligible.

Uncertainties of measured parameters are analyzed using the method introduced by Moffat [46]. Pressure was measured with an uncertainty of ±0.1% based on instrumentation error. The volume flowrate was measured with two sources of uncertainty: weight measurement and time control. We used a precise digital balance whose uncertainty could be omitted (±0.1 g precision within max. 4200 g). A stopwatch was used for time measurement. For each measurement the time interval is more than 100 s with a human error within ±0.5 s. Thus we have an uncertainty of flowrate measurement of ±0.5%. Uncertainty of energy dissipation rate, according to Eq. (2), is calculated to be ±0.5%.

4.5. Micromixing time determination using IEM model

The IEM model, developed for plug flow equipments, is used to estimate micromixing time. Applying this model requires that two solutions flowing inside a reactor have the same flowing age starting from their initial contact, which is exactly our case. Molecular exchange between two solutions is assumed to happen at a same time constant as that of mixing time t_m. Solutions are treated separately by keeping the concentration evolution of each one using differential equations in Eq. (19).

$$\begin{aligned}\frac{dC_{k,1}}{dt} &= \frac{\overline{C}_k - C_{k,1}}{t_m} + R_{k,1}\\ \frac{dC_{k,2}}{dt} &= \frac{\overline{C}_k - C_{k,2}}{t_m} + R_{k,2}\\ \overline{C}_k &= \alpha C_{k,1} + (1-\alpha)C_{k,2}\end{aligned} \tag{19}$$

In Eq. (19), R denotes the change rate of concentration for species k in concerned stream by reaction, mol/(L s); t_m the exchange time constant, with the same value of mixing time, s; α the global volume flow proportion of solution 1, which is 0.5 in our case. $\overline{C}_k$ stands for the mean concentration of mixture, mol/L.

With a presumed value of t_m and known initial concentration of ions in each solution, these differential equations can be integrated numerically via second order Runge Kutta method (RK2). Integration process for one presumed t_m is shown in Fig. 3. An algorithm is developed accordingly in Matlab. Species concentrations are updated each iteration step with new concentration data. Mean concentration and kinetic data are updated accordingly. The whole integration process ends until acid is all consumed, i.e., concentration of H^+ approaches zero. Here we take 10^{-9} mol/L as the criterion for total consumption of H^+ (with initial C_{H^+} being 0.072 mol/L).

Special notes should be made on choosing an appropriate iteration time step h. The step h should be kept small especially in first several steps. This is to avoid using the same kinetic item R without updating new concentrations. With the reactions being second- and fifth-order, the item R changes rapidly with concentrations. In our case we kept a fixed value of time step h at 10^{-8} s. Other values larger than 10^{-8} s may result in unrealistic negative concentrations due to total consumption of reactants. Too small value of h should also be avoided since it will increase largely the number of iterative calculations.

Repeating the same procedure shown in Fig. 3 with different presumed t_m, we get different segregation indexes. Shown in Fig. 4 is the relation between segregation index and micromixing time under our concentration condition. Micromixing time could then be determined using this relation, with the value of segregation index obtained experimentally.

Micromixing time estimation through IEM model returns the quality of micromixing which can be compared even if tests were done with different concentrations. Segregation index however depends highly on the initial concentration of each solution. While researchers tend to use their own solution concentrations for

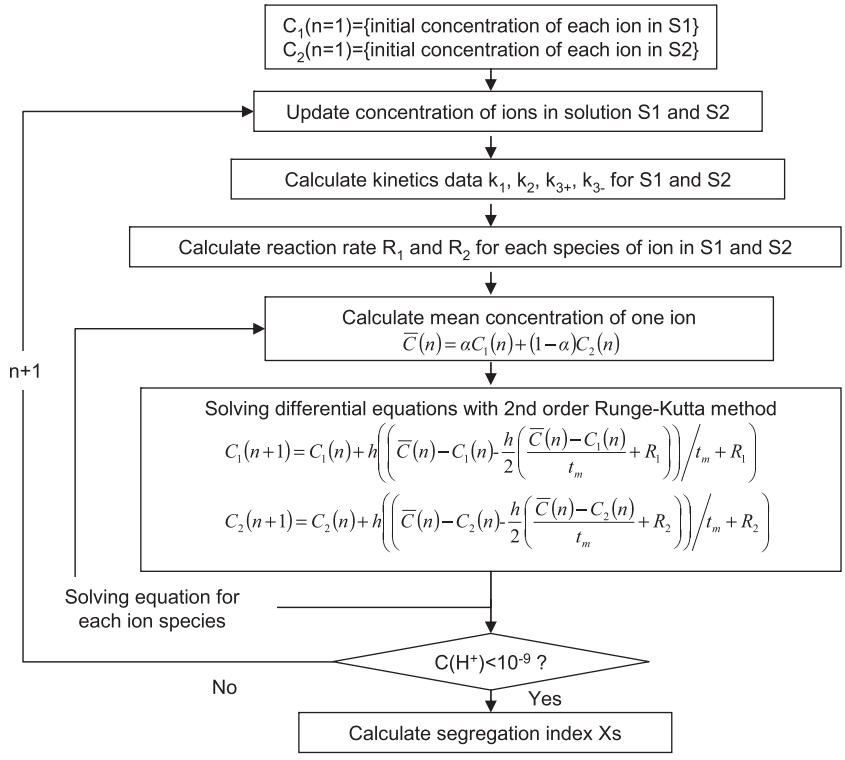

Fig. 3. Solving species concentrations of IEM model using 2nd order Runge Kutta method (RK2).

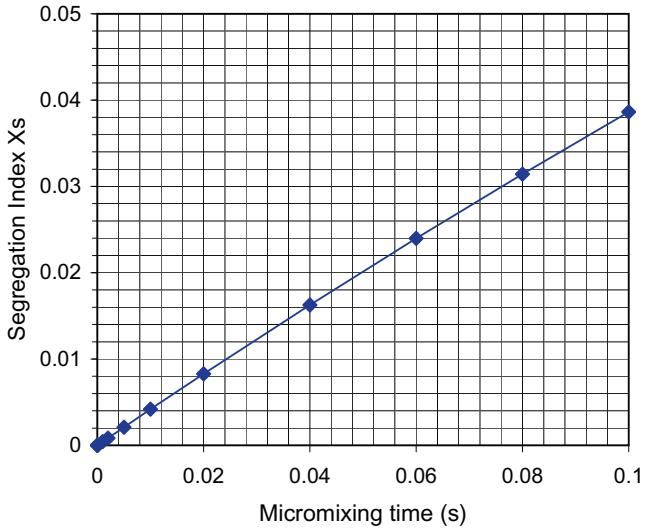

Fig. 4. Relation of micromixing time and segregation index under current research conditions. (S1:NaOH:0.125; H_3BO_3:0.25; KI:0.0116; KIO_3:0.00233, and S2:H_2SO_4:0.036. unit:mol/L.)

iodide/iodate reactions, direct performance comparison between different micromixers could only be done by comparing micromixing time other than by judging segregation index. Several studies have used this method for comparison [30,47]. Most recently in their review on mixing performance comparison [30], Falk and Commenge compared different continuous flow micromixers based on the IEM model.

5. Results and discussion

5.1. Energy dissipation rate

Experimentally obtained energy dissipation rate goes proportionally with the power of volume throughput in reactor, as shown in the double-log plot Fig. 5. Fitting exponent of this power curve is about $e_{diss,M2}$ = 3.68 for M2 and $e_{diss,M1}$ = 3.42 for M1, respectively, with unit for flowrate in mL/min and energy dissipation rate in W/kg.

Exponent of the relationship between energy dissipation rate and flowrate can reflect flow pattern. For Poiseuille flow in straight

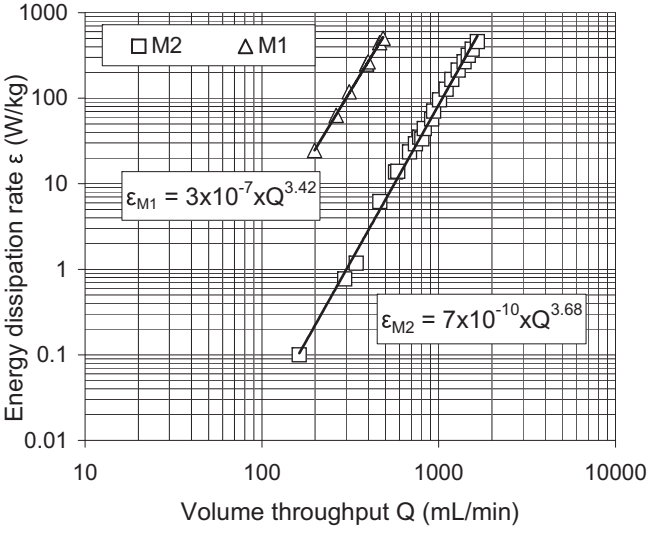

Fig. 5. Energy dissipation rate versus volume throughput.

Table 2
Flowrate of each inlet and corresponding Reynolds number inside reactor M2; *subscript*: *ch* – straight channel, *cs* – channel scale in the collector, scale number follows the index shown in Fig. 6a.

Flowrate of each inlet (mL/min)	Re_{ch}	Re_{cs1}	Re_{cs2}	Re_{cs3}	Re_{cs4}
300	396	623	1245	2490	4980
400	529	832	1663	3327	6653
500	659	1036	2072	4143	8287
600	793	1245	2490	4980	9960

tube, dissipation rate is proportional to the square power of velocity (thus the throughput), i.e., $e_{diss,laminar,pipe}$ = 2, as given by Eq. (3). The departure of our results from that of Hagen–Poiseuille flow comes from the distributor and collector parts. The same dimension in each bifurcation scale results in doubled velocity (and thus Re) after fluid merging. Shown in Table 2 are Re numbers inside the channels and at different scales of collector for M2. Under the studied flowrates, flow pattern in straight parallel channels is always laminar. While in the collector part, especially in channels of higher scales, flow pattern turns to be turbulent. Various local resistances like merging of two fluids and elbow flow contribute significantly to the total pressure loss too. Regarding global energy dissipation rate for turbulent flow, with local resistances taken into account, we have an exponent $e_{turbulent+local} \geqslant 3$. This indicates in our case that most pressure loss happens in the final collecting part where strong turbulence and flow collision take place.

5.2. Global mixing characteristics

Fast mixing happens at high flowrate, which can be observed directly from color evolution in collection part in Fig. 6. Fluids impinge at each contacting in the arborescent collector. Strong impingements generate higher turbulence and thus better mixing.

Within the studied flowrates (from 300 mL/min to 600 mL/min each inlet), complete mixing is only observed in collector. Straight channels after T-mixer contribute a little for the mixing, especially when flowrates are high. However channels are not sufficient to achieve complete mixing within their length. For small flowrates as shown in Fig. 6a, three impingements of the mixture inside arborescent collector are needed to achieve complete mixing. Less impingement is needed for high flowrates. As in the case of 600 mL/min for both inlets in Fig. 6d, fluids flowing out of channels are uniform in color only after the first impingement in collector. Complete mixing may even be achieved within straight channels when flowrate is further augmented (higher than 600 mL/min). We can draw the conclusion that, under our experimental conditions, mixing happens mainly by fluids impingement in collector part. Straight channels have marginal contribution to mixing, especially at low flowrates.

The same conclusion could be reflexed from analyzing Reynolds number of flow, as listed in Table 2. We notice that the flow changes from laminar regime to turbulent regime inside the collector, implying that mixing is enhanced in the collector part by turbulence. Meanwhile flow inside the channels is laminar. Mixing inside the channels thus is driven mainly by diffusive transfer.

The study of pH indicator visualization gives a general knowledge of mixing mechanism inside our reactor. Contacting fluids through a T-mixer under laminar flow condition requires a long channel due to the dominating mixing mechanism being diffusion. In such a T-mixer, future work needs to be done with the objective of enhancing the mixing within parallel channels. Channel geometry modifications (e.g. split-and-recombine structure; micro-fins inside channel other than smooth channel surface, etc.) are expected to be able to enhance mass transfer.

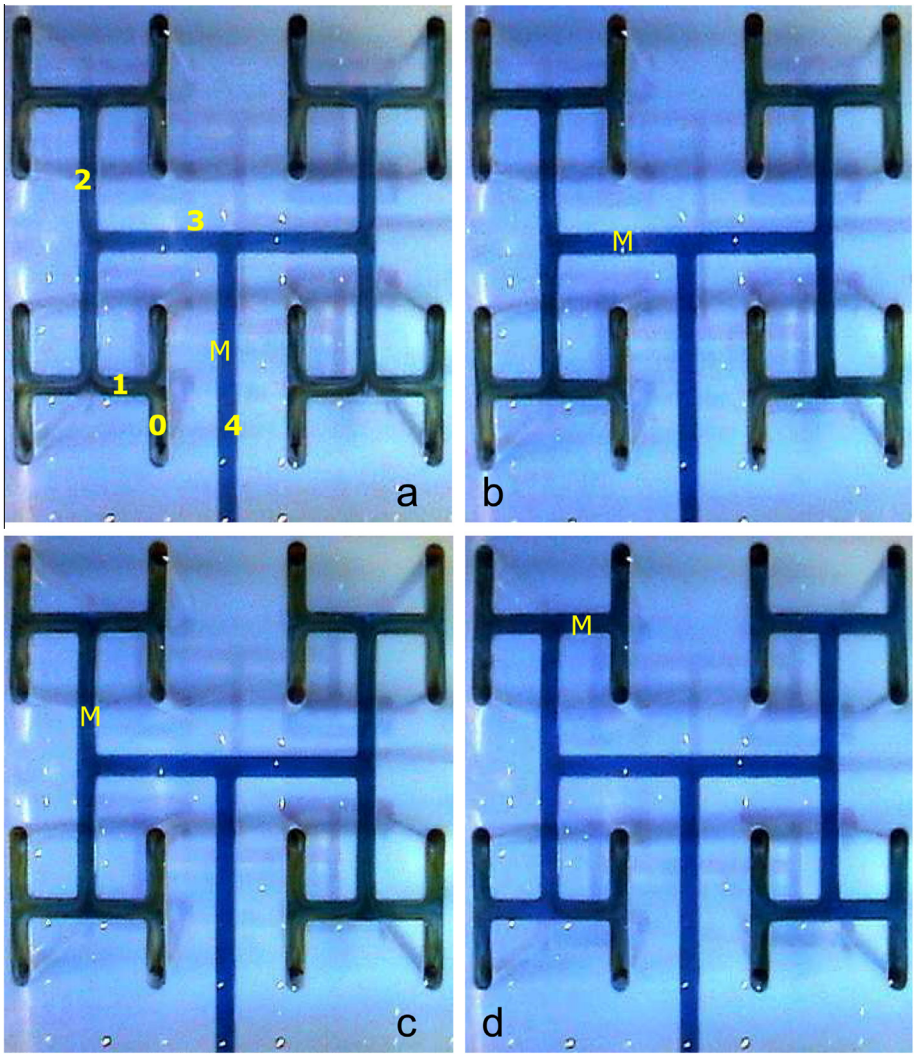

Fig. 6. Observation of mixing of BTB and Na_2HPO_4 solution. (Flowrate of each inlet: (a) 300 mL/min; (b) 400 mL/min; (c) 500 mL/min; (d) 600 mL/min; numbers 0–4 stand for scales of channels inside collector; M stands for fully mixed location.)

Uniformity of flow distribution between channels could also be reflected qualitatively by Fig. 6. From visualization of color evolution, we may observe that the flow inside the collector are quite symmetrical for branches at the same scale.

This qualitatively symmetrical observation indicates that for every channel, fluid from T-junction is a mixture of two solutions with a volumetric proportion of about 1:1. Despite the different color evolution for various throughputs, the symmetry feature does not change. This implies that under our tested conditions, fluids are distributed uniformly among 16 channels by designed arborescent structures.

However it has to be noted that the pH visualization result only gives a general idea of distribution and mixing. Maldistribution and its influence on mixing cannot be quantitatively shown in the photos.

5.3. Segregation index

Segregation indexes of both reactors decrease with the increase of volume throughput, as shown in Fig. 7. Reinforced fluid impingement and turbulence reduce the side redox reaction (R2) so that X_S becomes smaller at high flowrates. This result fits well with the pH indicator visualization experiment since high flowrate pushes fast mixing.

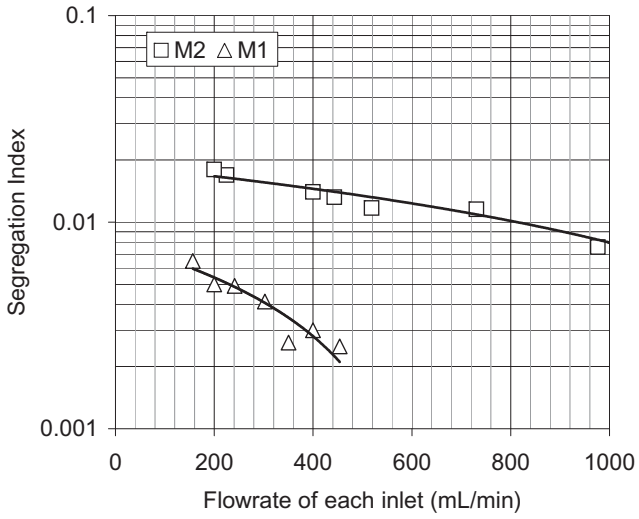

Fig. 7. Segregation index of M1 and M2 versus flowrates to each inlet.

Comparing the segregation index between M1 and M2, we observe an improved micromixing performance by reducing the size

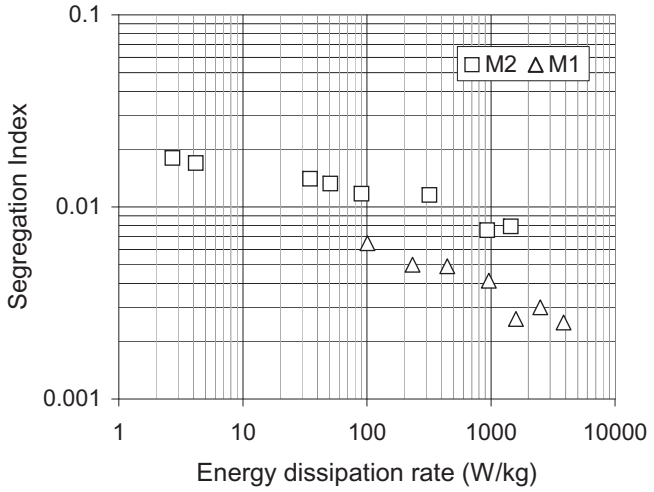

Fig. 8. Segregation index with energy dissipation.

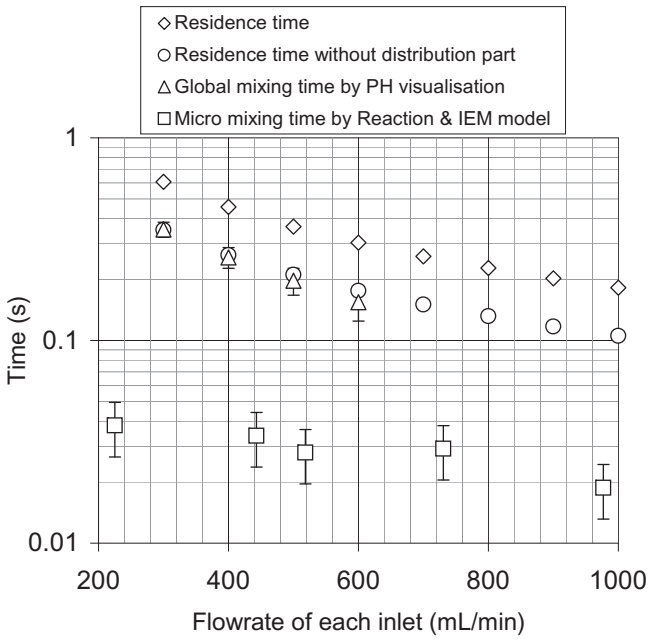

Fig. 9. Comparison of global mixing time, micromixing time and residence time under various flowrates for M2. (Estimation of mixing time by two methods: pH indicator visualization which gives global mixing time and, iodide/iodate reaction combined with IEM model which gives micromixing time; residence time is calculated with volume throughput and internal volume, with or without considering the volume of distributor.)

of reactor. At around 200–400 mL/min flowrate for each inlet, X_S for M2 varies from 0.017 to 0.014, while the value for M1 varies from 0.005 to 0.003. This implies that M1 is much more efficient for mixing than M2 at the same flowrate.

M1 is also preferable than M2 in terms of better mixing quality at a specific pumping power consumption. Shown in Fig. 8 is the variation of segregation index versus energy dissipation rate. With pumping power consumption of about 1000 W per kilogram of product (mixture of two inlet fluids, volumetric throughput is 600 mL/min for M1 and 2000 mL/min for M2 accordingly), X_S of M1 and M2 are 0.004 and 0.008, respectively. This indicates that by consuming the same pumping power for one kilogram of product, M1 offers a better mixing performance hence better quality of product than M2.

By putting several M1 in parallel, we can obtain the same volumetric throughput as M2, but with better mixing performance. Advantages of process intensification by miniaturization are clearly illustrated here.

It is worth noting the pressure drop characteristics at high throughputs. For M1 at a volumetric throughput of 600 mL/min (corresponding Reynolds number in channel is 793), total pressure drop is calculated to be 1.44 bar. For M2, at a throughput of 2000 mL/min (corresponding Reynolds number in channel is 1321), total pressure drop is 1.79 bar.

5.4. Global and micromixing time

Segregation index by reaction is used in IEM model to estimate micromixing time. For M2 this micromixing time is compared with global mixing time estimated by pH indicator visualization, as shown in Fig. 9. An uncertainty of 30% is concluded on micromixing time from using IEM model according to Falk and Commenge [30]. Regarding to global mixing time, the maximum uncertainty comes from the determination of mixing location. This maximum error is determined in such a way that the mixing point locates at the outlet of collector. Both of the two uncertainties are marked as error bars in Fig. 9.

Both global and micromixing time decrease with increasing flowrate, however not by the same rate. Global mixing time decreases proportionally with the increase of flowrate, at a rate much faster than that of micromixing time does. At a flowrate of 300 mL/min for each inlet, global mixing time and micromixing time are 0.35 s and 0.04 s respectively. While by increasing the flowrate to 600 mL/min, we get a global mixing time of 0.15 s and micromixing time of 0.03 s. At low flowrates, global mixing time can be 10 times longer than micromixing time; however at high flowrate this difference becomes smaller.

The difference between global mixing time and micromixing time may be explained by different mechanisms of mixing. As explained above, macro, meso and micromixing make up the whole mixing process. From our results, by increasing flowrate we enhanced the first two steps of mixing, i.e., macroturbulence and mesoflow stretching. The micromixing (say diffusive mass transfer) was also improved, but less sensible compared with the two other mechanisms.

Fig. 9 also shows residence time and residence time without considering distribution part. Residence time is theoretically calculated as the ratio of internal volume (with or without distributor volume) and total volume throughput, with the assumption of plug flow. Under the flowrates studied, residence time through the reactor M2 varies from 0.6 s to 0.3 s. Considering only mixing, the residence time without distribution part varies from 0.35 s to 0.17 s, indicating that fluids take more than 40% of their residence time for distribution.

Considering the residence time without distribution part and the global mixing time, we only observe a minor difference at high flowrate. The channels and collector are thus both occupied to achieve complete mixing before the fluid running out . At flowrate of 600 mL/min for each inlet, the global mixing time is 0.16 s and that of residence time without distributor is 0.17 s, meaning that 0.01 s is used for collecting product.

Micromixing time is much shorter than residence time, implying that micromixing happens within a very short time scale.

Finally it has to be made clear that both micromixing time and global mixing time estimations give the reliable orders of magnitude but not the precise values. Micromixing time estimation has an uncertainty of 30%, and that of global mixing time is 20%.

6. Discussion on mixing performance

6.1. Effective mixing volume

With pH indicator visualization it is possible to roughly estimate the effective mixing volume inside M2, counted from T-mixer to complete mixing locations (shown in Fig. 6). Collector contributes to mixing and thus is considered as effective mixing volume, whereas two distributors are not included. Shown in Fig. 10 are original geometric volume and effective mixing volume at various flowrates.

We observe that the whole volume of channels and partial volume of collector is needed to achieve complete mixing at studied flowrates. The smaller the throughput, the more volume of collector is used for mixing. Designed volume for distributor, channels and collector are 2.56 mL, 2.61 mL and 0.91 mL, respectively (as shown in left side of Fig. 10). With distributor volume being the same (2.56 mL) for various flowrates, effective mixing volume changes. At a flowrate of 500 mL/min for each inlet , the effective mixing volume is 3.28 mL. This value is the sum of channels volume and a big portion (0.67 mL out of 0.91 mL) of collector volume. At lower flowrate like in the case of 300 mL/min for each inlet , most part of the collector volume is used for mixing.

The effective mixing volume shows one weakness of our reactor: the designed heat exchanger is not well located around the mixing volume. Heat exchanger is only designed around parallel channels but not in the collecting part. In this case the reactor could only be used as a static micromixer. Reducing the length needed to achieve complete mixing inside the channels, or adding heat exchange for the collector part may be solutions for a proper heat exchanger reactor design.

6.2. Mixing performance comparison

With estimated micromixing time and dissipation rate, we are able to compare the mixing performance of our prototypes with other micro-structured designs reviewed by Falk and Commenge [30], as shown in Fig. 11. It should be noted that micromixing time of other structures are obtained with the same iodide/iodate scheme and using IEM model.

Both reactor M1 and M2 are found to be comparable in performance, under some flowrates, with certain micro-structured reactors. For M2, at low dissipation rates around 10 W/kg, its micromixing time corresponds with that of single T-mixer with channel dimension of around 800 μm [19] and that of IMTEK Tangential mixer with channel dimension 300 μm × 100 μm [39]. At higher energy dissipation rates, micromixing time of M1 is quite comparable (sometimes better than) several microdevices, including the triangular interdigital micromixer by Mikroglas (channel dimension 50 μm × 150 μm) [19], and Starlam micromixer by IMM (channel dimension ~100 μm) [40].

It is also interesting to compare the performance between M1 and M2 having different channel dimensions. By reducing the dimension of reactor by a half, the micromixing performance is improved. For example, by consuming 960 W/kg of pumping energy, micromixing time for M1 is 8 ms and that of M2 is 15 ms. This means that micromixing could be two times faster for reactor M1 than M2 without increasing energy dissipation. Rapid mixing under 5 ms can be realized using M1 by consuming 1500 W pumping power per kilogram of product.

Advantages of this mini-structured devices are attractive. Throughput of both M1 and M2 can be at the order of liter-per-minute, with a pressure drop at around 1 bar. This throughput is sometimes difficult for those microstructured devices to achieve. Problems like blocking usually found for micro-structures may be avoided with millimetric design. If conventional machinery methods can be used for fabrication, a good compromise between cost and performance would then be achieved.

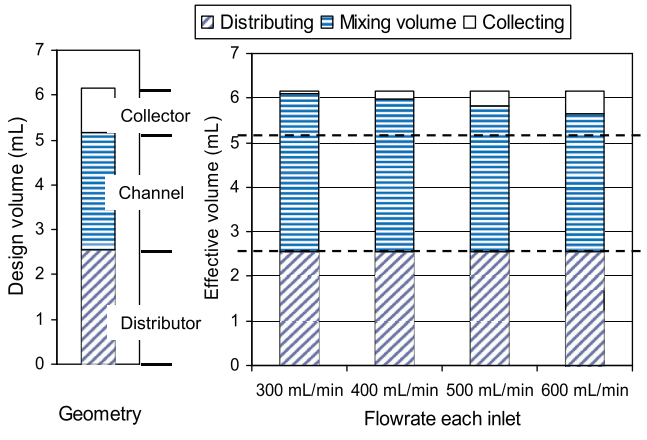

Fig. 10. Effective mixing volume at various flowrates and original designed volume for M2. (*Geometry* means the design volume of distributor, channels, and collector; flowrate is for single inlet.)

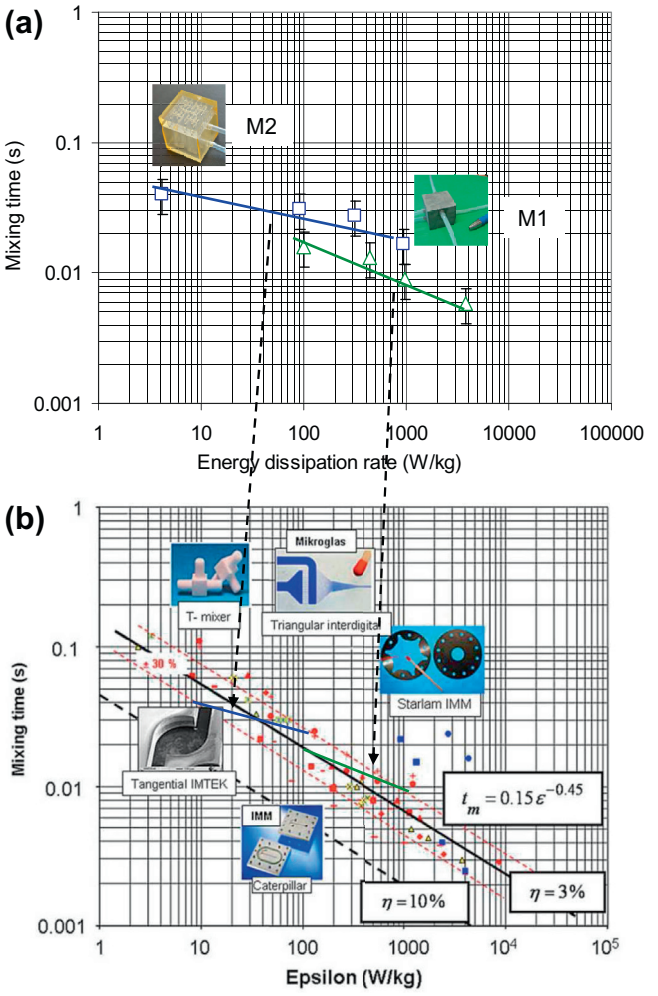

Fig. 11. Comparison of mixing time evolution with dissipation rate. ((a) Performance of our design M1 and M2; (b) Performance of some micromixers reviewed by Falk and Commenge [30]; Figure reproduced with permission.)

7. Conclusion

A high throughput, multi-channel, mini heat exchanger reactor with arborescent distributor was designed, fabricated and tested. Micromixing performance was tested using iodide/iodate reaction method. Micromixing time was estimated using IEM method with experimentally obtained segregation index. Global mixing visualization is realized using pH indicator BTB.

pH indicator visualization shows that uniform flow distribution and complete mixing are obtained using arborescent distributor and collector. Multi-collision of fluid in arborescent collector is shown to be quite helpful for mixing. Turbulent impingement of fluids enhances mass transfer so that rapid mixing can be realized.

From the micromixing characterization we found our millimetric design comparable, in terms of micromixing performance, to some micrometer products of IMM, Mikroglas, etc., but with higher throughput. This confirms the fact that we are not always obliged to search for micro-scale dimension only for obtaining a better mixing performance [48]. Other criteria (technical, economic, etc.) should be considered, in order to determine an appropriate dimension scale for a specific application. Millimeter-scale structures (sometimes called meso-scale structures), if properly designed, could have good mixing performance without increasing much pumping power consumption. High throughput can also be achieved by numbering-up of mini-channels, using arborescent type distributor and collector for uniform flow distribution.

Several drawbacks also exist for the current design. One of them is that mixing takes place mainly at the collector part, while heat exchanger is designed only for straight channels. Temperature control during endothermic/exothermic processes might be ineffective. Another drawback is that the geometries of arborescent distributor and collector are not optimized. No scaling relation was established for the channel size between different scales of the arborescent structure. The same characteristic channel size results in different flow patterns: laminar flow in straight channels, while strong turbulent flow in higher scales of distributor and collector. As we already discussed that turbulence in collector enhances mixing, turbulence in distributor however only results in unnecessary consumption of pumping power.

Our ongoing works are focused on the modification of geometry for better mixing and lower pressure drop. Split-and-recombine design, or nozzle design at T-junctions are expected to improve the mixing within straight channels. The shape of arborescent distributor/collector may also be optimized for a reduced pressure drop. Species distribution among the channels will be studied quantitatively using species transportation calculation in simulation. Residence time distribution may be used to quantitatively investigate this issue experimentally. A further goal is to study the integration of heat exchange function for some endothermic or exothermic reactions.

Acknowledgments

Authors would like to thank the financial support from the French authority Ministère de l'Enseignement Supérieur et de la Recherche. Technical supports from Thierry Goldin and Jonathan Outin in LOCIE, Polytech'Annecy-Chambéry, are gratefully appreciated.

References

[1] A. Stankiewicz, J.A. Moulijn, Process intensification: transforming chemical engineering, Chem. Eng. Progr. 96 (1) (2000) 22–34.
[2] T. Van Gerven, A. Stankiewicz, Structure, energy, synergy, time – the fundamentals of process intensification, Ind. Eng. Chem. Res. 48 (5) (2009) 2465–2474.
[3] J.C. Charpentier, Process intensification by miniaturization, Chem. Eng. Technol. 28 (3) (2005) 255–258.
[4] J.M. Commenge, L. Falk, J.P. Corriou, M. Matlosz, Analysis of microstructured reactor characteristics for process miniaturization and intensification, Chem. Eng. Technol. 28 (4) (2005) 446–458.
[5] C. Jiménez-González, P. Poechlauer, Q.B. Broxterman, B.S. Yang, D. am Ende, J. Baird, C. Bertsch, R.E. Hannah, P. Dell'Orco, H. Noorman, S. Yee, R. Reintjens, A. Wells, V. Massonneau, J. Manley, Key green engineering research areas for sustainable manufacturing: a perspective from pharmaceutical and fine chemicals manufacturers, Org. Process Res. Dev. 15 (4) (2011) 900–911.
[6] J.M. Commenge, L. Falk, J.P. Corriou, M. Matlosz, Optimal design for flow uniformity in microchannel reactors, AIChE J. 48 (2) (2002) 345–358.
[7] M. Saber, J.M. Commenge, L. Falk, Rapid design of channel multi-scale networks with minimum flow maldistribution, Chem. Eng. Process. Process Intensification 48 (3) (2009) 723–733.
[8] M. Saber, J.M. Commenge, L. Falk, Microreactor numbering-up in multi-scale networks for industrial-scale applications: impact of flow maldistribution on the reactor performances, Chem. Eng. Sci. 65 (1) (2010) 372–379.
[9] J. Yue, R. Boichot, L. Luo, Y. Gonthier, G. Chen, Q. Yuan, Flow distribution and mass transfer in a parallel microchannel contactor integrated with constructal distributors, AIChE J. 56 (2) (2010) 298–317.
[10] S.K. Ajmera, C. Delattre, M.A. Schmidt, K.F. Jensen, Microfabricated cross-flow chemical reactor for catalyst testing, Sens. Actuators B: Chem. 82 (2–3) (2002) 297–306.
[11] S.M. Senn, D. Poulikakos, Tree network channels as fluid distributors constructing double-staircase polymer electrolyte fuel cells, J. Appl. Phys. 96 (1) (2004) 842–852.
[12] C. Amador, A. Gavriilidis, P. Angeli, Flow distribution in different microreactor scale-out geometries and the effect of manufacturing tolerances and channel blockage, Chem. Eng. J. 101 (1–3) (2004) 379–390.
[13] J. Gradl, W. Peukert, H. Bockhorn, D. Mewes, H.J. Warnecke, Characterization of micromixing for precipitation of nanoparticles in a T-mixer, in: Micro and MacroMixing: Analysis, Simulation and Numerical Calculation, Heat and Mass Transfer, Springer, Berlin Heidelberg, 2010, pp. 105–124.
[14] F. Schwertfirm, J. Gradl, H.C. Schwarzer, W. Peukert, M. Manhart, The low Reynolds number turbulent flow and mixing in a confined impinging jet reactor, Int. J. Heat Fluid Flow 28 (6) (2007) 1429–1442.
[15] A.D. Stroock, S.K.W. Dertinger, A. Ajdari, I. Mezic, H.A. Stone, G.M. Whitesides, Chaotic mixer for microchannels, Science 295 (5555) (2002) 647–651.
[16] A. Lehwald, S. Leschka, K. Zähringer, D. Thévenin, Fluid dynamics and mixing behavior of a static mixer using simultaneously particle image velocimetry and planar laser-induced fluorescence measurements, in: 14th International Symposium on Applications of Laser Techniques to Fluid Mechanics, Lisbon, Portugal, 2008.
[17] A. Lehwald, S. Leschka, D. Thévenin, K. Zähringer, Experimental investigation of a static mixer for validation of numerical simulations, in: Micro and MacroMixing: Analysis, Simulation and Numerical Calculation, Springer, Berlin Heidelberg, 2010, pp. 227–243.
[18] G. Pan, H. Meng, Experimental study of turbulent mixing in a tee mixer using PIV and PLIF, AIChE J. 47 (12) (2001) 2653–2665.
[19] S. Panić, S. Loebbecke, T. Tuercke, J. Antes, D. Bošković, Experimental approaches to a better understanding of mixing performance of microfluidic devices, Chem. Eng. J. 101 (1–3) (2004) 409–419.
[20] P. Guichardon, L. Falk, Characterisation of micromixing efficiency by the iodide-iodate reaction system. Part I: Experimental procedure, Chem. Eng. Sci. 55 (19) (2000) 4233–4243.
[21] J.R. Bourne, S. Yu, Investigation of micromixing in stirred tank reactors using parallel reactions, Ind. Eng. Chem. Res. 33 (1) (1994) 41–55.
[22] J.R. Bourne, R.V. Gholap, An approximate method for predicting the product distribution of fast reactions in stirred-tank reactors, Chem. Eng. J. Biochem. Eng. J. 59 (3) (1995) 293–296.
[23] C.H. Phillips, G. Lauschke, H. Peerhossaini, Intensification of batch chemical processes by using integrated chemical reactor-heat exchangers, Appl. Therm. Eng. 17 (8–10) (1997) 809–824.
[24] C.H. Phillips, K.T. Symonds, Development of a novel compact heat exchange reactor, in: The 3rd International Conference on Process Intensification, Antwerp, Belgium, vol. 71, 1999.
[25] B.M. Walker, Einfluss der Temperatur-Segregation auf die Selektivität rasch ablaufender Reaktionen, Ph.D. thesis, Eidgenössische Technische Hochschule Zürich, 1996.
[26] J. Nilsson, F. Sveider, Characterising Mixing in a HEX Reactor Using a Model Chemical Reaction. <www.chemeng.lth.se/exjobb/002.pdf> (accessed 01.04.12).
[27] J. Aubin, M. Ferrando, V. Jiricny, Current methods for characterising mixing and flow in microchannels, Chem. Eng. Sci. 65 (6) (2010) 2065–2093.
[28] M.C. Fournier, L. Falk, J. Villermaux, A new parallel competing reaction system for assessing micromixing efficiency – experimental approach, Chem. Eng. Sci. 51 (22) (1996) 5053–5064.
[29] J. Villermaux, L. Falk, A generalized mixing model for initial contacting of reactive fluids, Chem. Eng. Sci. 49 (24) (1994) 5127–5140.
[30] L. Falk, J.M. Commenge, Performance comparison of micromixers, Chem. Eng. Sci. 65 (1) (2010) 405–411.
[31] J.M. Commenge, L. Falk, Villermaux–Dushman protocol for experimental characterization of micromixers, Chem. Eng. Process. Process Intensification 50 (10) (2011) 979–990.

[32] D. Tondeur, L. Luo, Design and scaling laws of ramified fluid distributors by the constructal approach, Chem. Eng. Sci. 59 (8–9) (2004) 1799–1813.
[33] L. Luo, D. Tondeur, Multiscale optimization of flow distribution by constructal approach, China Particuology 3 (6) (2005) 329–336.
[34] L. Luo, D. Tondeur, H. Le Gall, S. Corbel, Constructal approach and multi-scale components, Appl. Therm. Eng. 27 (10) (2007) 1708–1714.
[35] L. Luo, Y. Fan, W. Zhang, X. Yuan, N. Midoux, Integration of constructal distributors to a mini crossflow heat exchanger and their assembly configuration optimization, Chem. Eng. Sci. 62 (13) (2007) 3605–3619.
[36] Y. Fan, R. Boichot, T. Goldin, L. Luo, Flow distribution property of the constructal distributor and heat transfer intensification in a mini heat exchanger, AIChE J. 54 (11) (2008) 2796–2808.
[37] D. Tondeur, Y. Fan, L. Luo, Constructal optimization of arborescent structures with flow singularities, Chem. Eng. Sci. 64 (18) (2009) 3968–3982.
[38] Z. Fan, X. Zhou, L. Luo, W. Yuan, Evaluation of the performance of a constructal mixer with the iodide-iodate reaction system, Chem. Eng. Process. Process Intensification 49 (2010) 628–632.
[39] N. Kockmann, T. Kiefer, M. Engler, P. Woias, Convective mixing and chemical reactions in microchannels with high flow rates, Sens. Actuators B: Chem. 117 (2) (2006) 495–508.
[40] Y. Men, V. Hessel, P. Löb, H. Löwe, B. Werner, T. Baier, Determination of the segregation index to sense the mixing quality of pilot-and production-scale microstructured mixers, Chem. Eng. Res. Des. 85 (5) (2007) 605–611.
[41] P. Guichardon, L. Falk, J. Villermaux, Characterisation of micromixing efficiency by the iodide-iodate reaction system. Part II: kinetic study, Chem. Eng. Sci. 55 (19) (2000) 4245–4253.
[42] Y. Su, G. Chen, Q. Yuan, Ideal micromixing performance in packed microchannels, Chem. Eng. Sci. 66 (13) (2011) 2912–2919.
[43] H. Monnier, A.M. Wilhelm, H. Delmas, The influence of ultrasound on micromixing in a semi-batch reactor, Chem. Eng. Sci. 54 (13–14) (1999) 2953–2961.
[44] H. Monnier, A.M. Wilhelm, H. Delmas, Influence of ultrasound on mixing on the molecular scale for water and viscous liquids, Ultrason. Sonochem. 6 (1–2) (1999) 67–74.
[45] D.A. Palmer, R.W. Ramette, R.E. Mesmer, Triiodide ion formation equilibrium and activity coefficients in aqueous solution, J. Solution Chem. 13 (9) (1984) 673–683.
[46] R.J. Moffat, Describing the uncertainties in experimental results, Exp. Therm. Fluid Sci. 1 (1) (1988) 3–17.
[47] A. Kölbl, M. Kraut, On the use of the iodide iodate reaction method for assessing mixing times in continuous flow mixers, AIChE J. 57 (4) (2011) 835–840.
[48] J. Jenck, Process intensification for fine chemicals and advanced materials: methodology and achievements, in: AIChE Process Development Symposium, Palm Springs, CA, USA, 2006.